Fragility of network-forming glasses: A universal dependence on the topological connectivity

D. L. Sidebottom

Phys. Rev. E **92**, 062804 — Published 2 December 2015

DOI: 10.1103/PhysRevE.92.062804

Fragility of network-forming glasses: A universal dependence on the topological connectivity.

D. L. Sidebottom

Physics Department, Creighton University, Omaha, NE 68152 USA

Abstract

The fragilities of over 150 different network-forming glass melts are shown to conform to a common dependence on just one parameter: the connectivity of the weakest network structure present in the associated glass solid. This includes both non-oxide network-forming chalcogenide melts as well as a variety of alkali oxide glasses and spans a broad range of connectivity, ϕ, from polymeric structures ($\phi = 2$) to over-constrained random networks with connectivities well in excess of the rigidity threshold ($\phi_C = 2.4$). A theoretical framework for the origin of this universal pattern is offered within the context of entropic models of the glass transition.

PACS# 64.60.aq, 61.20.-p, 61.43.Fs, 64.70.ph

I. Introduction

Advanced uses for amorphous solids include metallic glasses[1], semiconductor devices[2], solid state electrolytes[3], nuclear waste encapsulation[4], and bone replacement therapy[5]. Yet, in spite of a century of investigation, the glass transition through which most of these materials are formed remains an unsolved problem of condensed matter physics[6-8]. According to many[7-9], the key challenge of the glass transition lies in understanding the mechanism by which a supercooled liquid (SCL) solidifies without ordering - a mechanism in which both thermodynamics and kinetics appear to be intertwined. Unlike crystallization in which a fixed amount of entropy is removed in a first order transition, the SCL avoids ordering by virtue of an enormous increase in viscosity, η, whilst a comparable amount of entropy is lost *gradually* with cooling. This gradual loss of excess entropy (S_{ex}, the entropy in excess of the vibrational content present in the crystal) represents a steady decrease in *accessibility* of phase space that is limited by the viscosity.

In the potential energy landscape (PEL) picture that has become popular for describing protein folding[10-12] as well as the thermodynamics of SCLs[13-17], this inaccessibility is readily understood. The potential energy landscape is a representation of the potential energy surface as a function of the $3N$ coordinates of the N atoms that is characterized by hills and valleys separated by saddle points. As the system is cooled toward the glass transition point, it becomes trapped into ever smaller basins of the PEL and becomes unable to explore the configurations of neighboring basins owing to the intervening energy barrier[16,17]. The accessibility of phase space is, thus, also limited

by the molecular relaxation time of the SCL that limits the likelihood for transitions over these barriers. The relaxation time scales with the viscosity and, in the Adam-Gibbs model[18], can be expressed in terms of the excess entropy as

$$\eta = \eta_o \exp\left(B / TS_{ex}\right), \tag{1}$$

where η_o and B are constants. Although other models[19-21] have been proposed for the temperature dependence of the viscosity, the Adam-Gibbs model is most often cited and is supported by experiment[22,23]. In this model the kinetic slow down of the SCL is effectively driven by the decreasing entropy[24] and the divergence of the relaxation time is choreographed to coincide with the final loss of excess entropy, narrowly averting a potential "entropy catastrophe"[25] (where $S_{ex} < 0$) by enforcing a loss of ergodicity for all observers. In actual practice, the loss of ergodicity occurs when the relaxation time exceeds common laboratory timescales (≈ minutes) at the glass transition temperature T_g where one observes a step-like decrease in specific heat arising from the abrupt change in dS_{ex} / dT [26,27].

For more than 40 years, *fragility*[26] has served as the dominant means of classifying different glass-forming materials and has guided most theoretical efforts to connect glass-forming properties to structural bonding. The fragility is commonly quantified by the *fragility index* defined by the steepness of the viscosity in a scaled Arrhenius plot[26],

$$m = \left.\frac{d \log_{10} \eta}{d\left(T_g / T\right)}\right|_{T \to T_g}. \tag{2}$$

Fragile glasses ($60 < m < 150$) are largely populated by molecular liquids and polymers that owe their cohesive strength to van der Waal or ionic interactions that are long range

and non-directional[28]. By contrast, strong glasses ($17 < m < 30$) are typically network-forming oxides (e.g., SiO_2) that develop as a result of highly directional covalent or hydrogen[29] bonds that obey strict rules[30] regarding the numbers of bonds per atom (r). Fragility is an important metric of a SCL's glass-forming tendency that simultaneously characterizes the rate of viscosity increase and the rate of entropy decrease on approach to the glass transition temperature, T_g, from above[27]. This dual nature of the index m readily appears when Eq. (1) and Eq. (2) above are combined to obtain a *reduced* fragility[31]:

$$m^* = \left(m - m_o\right)/m_o = \left.\frac{d\left[S_{ex}\left(T\right)/S_{ex}\left(T_g\right)\right]}{d\left(T/T_g\right)}\right|_{T\to T_g} = \left.\frac{dS_{ex}^*}{dT^*}\right|_{T^*\to 1}, \qquad (3)$$

where $m_o = B\log_{10} e/T_g S_{ex}\left(T_g\right) \approx 17$ is the lower limit of fragility[28]. This relationship neatly captures the deep connection between kinetics and thermodynamics and explains why the fragility is so well correlated with the step increase in specific heat that accompanies the transition[27].

Because the bonds in network forming glasses (NFGs) are discrete and result in a well-defined network of covalent linkages between atoms, these materials provide an excellent platform for exploring inherent connections between fragility and the excess entropy of the SCL. The NFG structure can be pictured as a collection of balls connected by rods and discussed within the context of rigidity theory[32-34] and constraint counting[35,36] approaches which consider the competition between degrees of freedom (of the balls) and the growing number of linear and angular constraints posed by the rods. Rigidity is said to percolate[33] into existence when the degrees of freedom are balanced by an equal number of constraints and this occurs when the average number of bonds per

atom, $\langle r \rangle$, reaches 2.4. To date, many studies[37-40] of chalcogenide solids have reported extrema in both mechanical and thermal properties near this threshold, including a vanishing non-reversing heat flow measured by temperature-modulated differential scanning calorimetry (TMDSC) argued as evidence for an "intermediate phase"[39] of so-called *isostatic* (rigid but stress-free) networks that form over a narrow window of compositions near $\langle r \rangle = 2.4$. More importantly, thermodynamics can be easily incorporated into these structural models through the addition of thermally activated bond breaking or bond "excitation"[41]. These excitations can be introduced using a simple two state (intact or broken) model[41] or by employing more elaborate methods[36].

In this paper, we examine the fragility of over 150 network-forming glasses, including both oxide and non-oxide networks built from discrete covalent bonding. We demonstrate that the fragilities of these network-forming glasses are *universally* determined by a single mean field parameter: the connectivity of the weakest network. This weakest network is identified by coarse-graining over any rigid structural units that are present and is key to observing the universal pattern. A simple two state bond excitation model that incorporates both configurational and vibrational contributions to the excess entropy is shown to provide a theoretical framework for understanding this universal pattern.

II. Background

In Fig. 1 the reduced fragility for a series of chalcogenide glasses[37,38] of the form $Ge_xAs_xSe_{1-2x}$ is plotted as a function of $\phi = \langle r \rangle$, the average atomic bond number. With the addition of Ge and As, the average bond number increases from $\langle r \rangle = 2$ while

the fragility drops from $m^* \approx 4$ to a plateau of roughly $m^* = 1$ beyond the rigidity threshold at $\langle r \rangle = 2.4$. Quite remarkably, the fragility of a series of sodium phosphate glasses[42] exhibit precisely the same decrease but as a function of $\phi = \langle n \rangle$, where $\langle n \rangle$ is the average *bridging* oxygen *per network-forming cation* (here, the phosphor atom). As alkali are reduced from the metaphosphate ($NaPO_3$), $\langle n \rangle$ increases from $\langle n \rangle = 2$ to 3 and the fragility decreases from $m^* \approx 4$ to the same plateau and finally to $m^* \approx 0$ in P_2O_5. This pattern is repeated again for a series of aluminophophate glasses[43] as $\langle n \rangle$ is increased from $\langle n \rangle = 2$ by the introduction of aluminum oxide which enters the oxide network structure mainly in the form 6-fold coordinated AlO_6.

To understand the rationale for adopting $\langle n \rangle$ as an alternative measure of connectivity for the oxides, we highlight several important differences between chalcogenide and oxide networks. The O^{2-} anion may share a common chemistry with its companions (S^{2-} and Se^{2-}) in column six in the period table, but the manner in which it interacts with various network-forming cations (e.g., Si^{4+}, B^{3+}, P^{5+}, etc.) is markedly different and results in quite different physical properties of the glasses that are formed[6,29,43]. Oxide glasses, for example, have a larger bandgap than the chalcogenides and are transparent at visible wavelengths while many chalcognides are opaque and exhibit semiconducting properties. Chalcogenide networks are also more loosely bound than their oxide counterparts[44]. Owing to its smaller size, the O^{2-} anion has 50% greater "field strength" (ratio of the valence charge to ion radius) than either S^{2-} or Se^{2-} and is able to form stronger bonds with the network-forming cation. This stronger bonding is evident in Raman scattering where the vibrational modes of the oxides appear

at energies roughly twice that of the corresponding modes in the S and Se chalcogenides. The enhanced bonding of the O^{2-} anion to the cation restricts glass-forming oxides to form only at well-defined[30] stochiometric ratios (e.g., SiO_2, GeO_2, B_2O_3, etc.) unlike the chalcogenides that form glasses over a wide range of atomic compositions that permit the formation of homopolar bonds (e.g., Se-Se).

Thus, we believe the coincidence between the fragility of chalcogenides described by $\phi = \langle r \rangle$ and that of oxides described by connectivity $\phi = \langle n \rangle$ is not fortuitous, but indicates a structural equivalence with respect to how these two classes of NFGs deform under the sort of low frequency stress that defines the viscosity (and in turn determines the fragility). This equivalence is most apparent for the case of $\phi = 2$ where both systems are, topologically speaking, equivalent *polymeric* materials: Se is a glass of long chains of Se atoms and $NaPO_3$ is a glass of long chains of PO_4 tetrahedra. Both systems undergo an increasing connectivity as a result of crosslinking or "polymerization". For the chalcogenide, it is the addition of Ge and As that increases the mean connectivity via the introduction of more "rods" between the atomic "balls". But for the phosphates, the short-range order (SRO) is strictly preserved[30]: homopolar bonding (e.g., P-P or O-O) is absent and the stronger bonding of the O^{2-} anion with the network-forming cation promotes a *stiffening* of the PO_4 tetrahedral unit relative to the interconnecting bridging oxygen bonds[30]. Degrees of freedom *inside* the tetrahedral unit are internalized and cease to participate in the sort of low frequency deformations that define the viscosity. This causes the tetrahedral units to assume the role of "balls" interconnected by a network of bridging oxygen "rods". In effect, we have argued[43-46] that the common pattern in Fig. 1 reflects an important *coarse graining* of the network wherein *rigid structural units*

(RSUs), like the oxide tetrahedron, are treated as autonomous objects *inter*-connected together by relatively weaker linkages.

A rationale for the specific shape of the master curve in Fig. 1 is lacking, but the curve does lend itself well to division into two separate contributions illustrated by the dashed lines in the figure. The rapid decrease at small ϕ is best captured using a quadratic function, $m_C^* \approx \left(\phi_C - \phi\right)^2$, that vanishes near $\phi_C = 2.4$. In light of how m^* is directly related to dS_{ex}^* / dT^* in Eq. (3), we suspect this contribution is dominated by the configurational part of the excess entropy since it appears to vanish beyond the rigidity threshold when the degrees of freedom are exceeded by the bonding constraints. The second contribution, that remains active above $\phi_C = 2.4$ in those over-constrained NFGs that are populated by redundant constraints, is adequately described by a Gaussian centered around $\phi_o = 2.6$, $m_V^* \approx \exp\left(-\left(\phi - \phi_o\right)^2 / \sigma^2\right)$ and is presumably dominated by the vibrational contribution[27,47] to the excess entropy.

Included in Fig. 1 are the fragilities of several alkali borate glasses plotted as a function of the average bridging oxygen per B atom, $\phi = \langle n \rangle$. In B_2O_3, all B are 3-coordinated and this coordination increases with addition of alkali oxide over the range of compositions shown[48]. Clearly the fragility now increases with increasing $\langle n \rangle$ in contradiction to all the other systems shown in the figure. The decrease of fragility with crosslinking of the polymeric glasses discussed previously is anticipated on approach toward the rigidity threshold since excess entropy should diminish as constraints begin to overtake degrees of freedom. But the increase of fragility in the borates suggests this same entropy can somehow be returned by adding more, redundant, bonds to an already

highly over-constrained network whose degrees of freedom have long since been vanquished. The resolution to this contradiction resides in the peculiar intermediate range order (IRO) of the alkali borate system[45] that contains RSUs at length scales beyond that of the SRO[48,49]. In amorphous boron oxide, some 65 to 75% of the boron atoms participate in 3-membered "boroxol" rings[49] illustrated in Fig. 1. A sharply defined Raman mode identifies the ring as a RSU and an additional level of coarse graining must be applied to determine the mean connectivity of the lattice of weakest links (the ϕ-network) relevant to the fragility. Although an isolated BO_3 unit has $n = 3$ connecting vertices, one of the two vertices of a BO_3 unit participating in a boroxol ring is (topologically) redundant and this reduces the effective connectivity of the BO_3 unit to $n = 2$. Treating the BO_3 units in these rings (and other RSUs that form at higher alkali content[49]) in this way, coarse graining was applied[45] to arrive at $\phi = \langle n_{IRO} \rangle$ describing the network of weakest links whose fragility (see Fig. 1) is seen to again conform to the master curve.

III. Analysis

In the present work, we return to the chalcogenides to consider a wider range of compositions of the form $Ge_xAs_y(S,Se)_{1-x-y}$ formed by crosslinking either Se or S with Ge and As. Published data[37,38,50-52] for some 74 chalcogenide glasses have been collected for analysis and the compositional range is shown in the ternary diagram in Fig. 2. These include glasses on either side of the stoichiometric ratio (indicated by the join between $Ge(S,Se)_2$ and $As_2(S,Se)_3$) whose chalcogen contents are characterized[52] by the deviation from the stoichiometric join, $z = 1 - 3x - 2.5y$. Glasses with $z > 0$ are rich in

chalcogen element while glasses with $z < 0$ are deficient. Starting from the chalcogenide corner of the ternary diagram, the network structure evolves from one of long -Se- chains that are infrequently crosslinked to compositions near the stoichiometric join ($z = 0$) where these chains have shortened substantially. Here, homopolar bonds of the form Se-Se are rare[53] and heteropolar bonds (Se-Ge, Se-As) are common while beyond the join ($z < 0$), the deficiency of Se atoms forces the appearance of unfavorable metal-metal bonds (Ge-Ge, As-As, Ge-As).

For all these glasses, the average number of bonds per atom can be calculated as $\langle r \rangle = 4x + 3y + 2(1 - x - y)$ and the fragility is plotted as a function of $\phi = \langle r \rangle$ in the inset of Fig. 3 together with the master curve developed by the oxide glasses discussed above. For compositions between $\langle r \rangle = 2$ and $\langle r \rangle \approx 2.5$, the fragility agrees favorably with the master curve. However, in every instance for $\langle r \rangle > 2.5$, the fragility begins to increase with increasing $\langle r \rangle$ in already over-constrained networks mimicking the same contradiction that plagued the alkali borates. Intermediate range order has been reported[53-58] in these chalcogen-deficient ($z < 0$) glasses and the two forms of RSUs that develop (illustrated in Fig. 2) are the likely culprit for the contradictory increase in fragility with increasing $\langle r \rangle$. In the As-rich regions, Raman spectroscopy has identified the formation of As_4Se_3 and As_4Se_4 molecules in roughly equal abundance[54,56]. These molecules are fully detached from the network and, as Aitken rightly noted[59], provide no connectivity for it. In the Ge-rich regions, Se deficiency leads to an evolution of $GeSe_{4/2}$ tetrahedra from corner sharing to edge-sharing (ES) configurations as evidenced by the growth of a discernable Raman mode associated with vibrations of the 2-membered ring that is created[57,58]. Much like the boroxol rings discussed earlier, the

ES $GeSe_{4/2}$ units form RSUs in which each Ge has a redundant bond (r is thus reduced from 4 to 3) and each Se provides no connectivity to the external network ($r = 0$).

Both of these RSUs produce a reduction in the coarse-grained connectivity and could potentially resolve the conundrum if the fractions of Se in molecules, $f_{Se}^{M}(x,y)$, and in ES units, $f_{Se}^{ES}(x,y)$, were accurately known. A glass of N atoms contains $N_{Ge} = xN$ Ge atoms, $N_{As} = yN$ As atoms, and $N_{Se} = (1-x-y)N$ Se atoms. An equal number of Ge and Se atoms, $N_{Ge}^{ES} = N_{Se}^{ES} = f_{Se}^{ES}(x,y)N_{Se}$, would occur in ES units while free molecules would consume $N_{Se}^{M} = f_{Se}^{M}(x,y)N_{Se}$ Se atoms and $N_{As}^{M} = \frac{8}{7} f_{Se}^{M}(x,y)N_{Se}$ arsenic atoms (given the equal abundance of As_4Se_3 and As_4Se_4). Combining these distributions with the reduced bond numbers described above, the coarse-grained ϕ-network would be given would be:

$$\begin{aligned}
\phi = \langle r_{IRO} \rangle &= \frac{1}{N}\left\{4\left(N_{Ge} - N_{Ge}^{ES}\right) + 3\left[\left(N_{As} - N_{As}^{M}\right) + N_{Ge}^{ES}\right] + 2\left(N_{Se} - N_{Se}^{ES} - N_{Se}^{M}\right)\right\} \\
&= \frac{1}{N}\left\{4\left(N_{Ge} - f_{Se}^{ES}N_{Se}\right) + 3\left(N_{As} - \frac{8}{7}f_{Se}^{M}N_{Se} + f_{Se}^{ES}N_{Se}\right) + 2\left(N_{Se} - f_{Se}^{ES}N_{Se} - f_{Se}^{M}N_{Se}\right)\right\} \\
&= 4x + 3y + 2(1-x-y) - \left\{3f_{Se}^{ES}(x,y) + \frac{38}{7}f_{Se}^{M}(x,y)\right\}(1-x-y) \\
&= \langle r \rangle - \left\{3f_{Se}^{ES}(x,y) + \frac{38}{7}f_{Se}^{M}(x,y)\right\}(1-x-y)
\end{aligned} \tag{4}$$

Raman studies[54-57] provide mainly *qualitative* evidence for the growth in numbers of RSUs along either of the two binaries. Along the As-Se binary, a linear increase in the Raman mode corresponding molecule formation is indicated and the value of $f_{Se}^{M}(x,y)$ is reported[54] to be as high as 40% in As_3Se_2. Similarly, the Raman mode associated with ES units increases in a linear manner[57] along the Ge-Se binary.

Otherwise, accurate values for the fractions $f_{Se}^{M}(x,y)$ and $f_{Se}^{ES}(x,y)$ throughout the ternary region are not known and so the coarse graining cannot be unambiguously applied. Instead, what we can do is test whether the coarse graining described in Eq. (4) is capable of transposing the errant fragility back onto the master curve using a reasonable model that can capture the linear increase in the numbers of RSUs seen experimentally with the least intervention. For the molecules, we adopt a simple linear dependence that involves only a single adjustable parameter:

$$f_{Se}^{M}(z,y)=\begin{cases}0 & z>0\\ B_{Se}^{M}\left(y/y_{\max}(z)\right)z=B_{Se}^{M}\left(2.5y/(1-z)\right)z & z<0\end{cases} \tag{5}$$

This linear dependence on *z* is augmented by an additional (linear) weighing that operates along any given join of fixed *z* to force molecule formation to be maximized at the As binary, $y_{\max}(z,x=0)=(1-z)/2.5y$, while vanishing at the Ge binary. An identical strategy is adopted for the fraction of Se in ES units:

$$f_{Se}^{ES}(z,x)=\begin{cases}0 & z>0\\ B_{Se}^{ES}\left(x/x_{\max}(z)\right)z=B_{Se}^{ES}\left(3x/(1-z)\right)z & z<0\end{cases} \tag{6}$$

Together with Eq. (4), the model is limited by just one parameter for each of the two RSU species (B_{Se}^{M} and B_{Se}^{ES}) and these have been independently adjusted to obtain a viable $\langle r_{IRO}\rangle$ that could transpose the errant fragility onto the master curve.

IV. Results

The result of coarse graining using values of B_{Se}^{M} = -0.4 and B_{Se}^{ES} = -0.7 is shown in Fig. 3. Despite the wide compositional range of the Se glasses, spanning from the As binary to very near the Ge binary, this single set of parameters is remarkably successful at

transposing the fragility back onto the master curve. Moreover, the values of $f_{Se}^{M}(x,y)$ and $f_{Se}^{ES}(x,y)$ produced by the model compare favorably with literature estimates. As an example, along the As-Se binary where Lucas[54] has reported $f_{Se}^{M}(z=-0.5, y=0.6) \approx$ 40%, the model favors a value of 20%. The agreement is not perfect, but the model prediction is considered reasonable as it is of a similar order of magnitude. Applied to the sulfide data, the same model requires values (B_S^M = -0.8 and B_S^{ES} = -1.3) that are roughly double those of the selenides, consistent with Aitken's qualitative assessment[59] that molecule formation is the "dominant structural component" in the sulfides near the As-S binary (i.e, implying that $f_S^M(z \approx -0.3, x \approx 0.1) \geq 50\%$).

Of the 74 compositions, just three data points (two open squares and one filled triangle in Fig. 3 at $m^* \geq 2.5$) deviate noticeably from the master curve. This deviation is expected and deserves a few brief comments. The last two compositions at the extremes of Se-deficiency in the As-Se binary are known[54] to contain As_4 molecules in addition to the As_4Se_3 and As_4Se_4 molecules discussed above. These As_4 molecules are not present at $y < 0.55$ and were omitted in formulating our single parameter model. Including the As_4 molecules would shift the $\langle r_{IRO} \rangle$ of these last two compositions only to lower values and, indeed, just 10% of As in As_4 is sufficient to achieve the needed adjustment for the datum corresponding to As_3Se_2. As for the other two errant data points in the sulphide system (open squares), it is reported that As_4S_4 and As_4S_3 molecules increase in numbers below $z = 0$ but, unlike the selenide system, these molecules abruptly *vanish* beyond $z < -0.3$[50,56]. If this cutoff of the molecule

formation were included, it produces precisely the needed shift of these two data points to larger $\langle r_{IRO} \rangle$ placing them onto the master curve.

V. Discussion

One finds in Fig. 3 a remarkably common pattern that develops for the fragility of over 150 oxide and non-oxide NFGs as a function of the mean field connectivity of weakest linkages obtained through coarse graining over rigid structural units. This includes most of the major oxides (borates, germanates and phosphates) and over 70 chalcogenide compositions. The universal curve indicates that it is the network of weakest links, the ϕ-network, that is relevant for the liquid's viscosity as this is the network that dictates the fragility. But how might we understand the origin of such a universal dependence given the relation of fragility to changing excess entropy found in Eq. (3)? In the following sections, we explore possible explanations.

We begin by applying the chain rule to Eq. (3):

$$m^* = \left. \frac{dS_{ex}^*}{dT^*} \right|_{T \to T_g} = \left. \frac{dS_{ex}^*}{d\phi} \frac{d\phi}{dT^*} \right|_{T \to T_g} . \tag{7}$$

The first term represents a measure of how much entropy gain is produced in the ϕ-network whenever ϕ increases by some small amount, regardless of whether the connectivity change is produced thermally or chemically. That is, $dS_{ex}^* / d\phi$ is *inherent* to the chemical structure of the NFG at a given composition. By contrast, the second term represents the action of thermal energy as a *catalyst* for disrupting the ϕ-network through the breaking and reformation of bonds. For this term, we appeal to a simple classical thermodynamic model for insight.

Two Level System Thermodynamics

Since the ϕ-network represents a structure of weakest level connections, it is not unreasonable to develop $d\phi / dT^*$ using the same two-level system approach[41,47] that was first advocated by Angell and Rao[41] over 40 years ago. All the ϕ-level bonds would then be treated as energetically equivalent and randomly "excited" by the thermal field. Every bond that is excited from its intact ground state to an excited broken state incurs a corresponding change in the Gibbs free energy, $\Delta G = \Delta H - T\Delta S$. The partition function contains just two terms and the (molar) fraction of intact (un-excited) bonds is given as $P_I = \left(1 + \exp\left(-\Delta G / RT\right)\right)^{-1}$. This probability is plotted in Fig. 4 for the fixed enthalpy ΔH = 2 kcal/mol at a series of ΔS between 1 to 7 cal/mol K and illustrates many of the points that were previously emphasized[41,47]. Firstly, the transition point (near 200 K, in this example) is determined by ΔH while ΔS largely influences the *rate* (i.e., $d\phi / dT^*$) at which the intact bond probability decreases at temperatures above the transition. Secondly, the bond probability varies in a linear fashion over some region just above the transition and, as highlighted in the inset, the slope of this linear region is roughly proportional to the value of ΔS which, by definition, equals $dS_{ex}^* / d\phi$. Since this slope is also proportional to the $d\phi / dT^*$, we draw from Eq. (7) the significant conclusion that the fragility depends entirely on the *inherent* sensitivity of excess entropy to changes in the connectivity of the network:

$$m^* \propto \left(\frac{dS_{ex}^*}{d\phi} \right)^2 . \qquad (8)$$

Thus, at least a conceptual framework is established for understanding the existence of a fragility master curve.

But what additional evidence might we provide to support this relation between *m** and $dS_{ex}^{*}/d\phi$? In the next section we explore the configurational entropy of a self-avoiding walk (SAW) polymer as it becomes progressively constrained by the sequential addition of crosslinks. This is a poor model for an actual NFG melt as it ignores the additional restrictions of inter-polymer entanglements present in the bulk. Nevertheless, it is an exactly solvable model that can be readily evaluated to demonstrate how $\left(dS_{ex}^{*}/d\phi\right)^2$ might reasonably be expected to decrease with increasing ϕ in a fashion similar to the initial decrease in *m** seen experimentally.

Self-Avoiding Walk Model

The enumeration of the possible conformations for a 3D self-avoiding walk is well documented[60-62] and numerical studies have shown that the number of possible conformations of a chain of *N* monomers, having a given end-to-end separation, follows a scaling law of the form:

$$W(N) = A\mu^{N}N^{-\delta}, \tag{9}$$

where *A* is an arbitrary constant while $\mu \approx 4.7$ and $\delta \approx 1.76$ in 3D. *W(N)* represents all the possible microstates for the chain consistent with its given end-to-end macrostate and the logarithm of this number is a precise measure of the configurational entropy of the chain. Now imagine that *i*-1 crosslinks are added the chain in such a way that the chain is equally subdivided by the crosslinks into *i* segments (as illustrated in Fig. 5). As far as the polymer is concerned, each crosslink imposes a constraint by fixing the location of

the corresponding monomer in the chain, thus reducing its possible conformations. Provided the resulting chain segments remain sufficiently long for the scaling law to apply to each individually, the total number of conformations of the entire chain with i-1 crosslinks would be:

$$W_i\left(N_i\right)=\left[A\mu^{N_i}N_i^{-\delta}\right]^i=\left[A\mu^{\left(N_1/i\right)}\left(N_1/i\right)^{-\delta}\right]^i \quad , \tag{10}$$

while the connectivity of the system would grow as

$$\phi=3\left(\frac{i-1}{N_1}\right)+2\left(1-\frac{i-1}{N_1}\right). \tag{11}$$

This connectivity changes by a small amount when i is incremented and the corresponding change in the configurational entropy can be directly evaluated as

$$\frac{dS_C}{d\phi}=\Delta S_{SAW}\propto\ln\left\{\frac{W_{i+1}\left(N_{i+1}\right)}{W_i\left(N_i\right)}\right\}=\ln A-i\delta\ln\left(\frac{i}{i+1}\right)-\delta\ln\left(\frac{N_1}{i+1}\right) \quad . \tag{12}$$

In Fig. 5, we have plotted ΔS_{SAW} against ϕ for the case of N = 100. The curve can be shifted vertically by the arbitrary parameter A (here chosen to be A = 1) but is otherwise largely independent of the actual value of N used. When crosslinks are initially added, the entropy decreases ($\Delta S_{\mathrm{SAW}} < 0$). This decrease does not remain fixed with increasing connectivity, but becomes ever smaller in magnitude as the polymer chain is increasingly constrained. The change in the entropy becomes vanishingly small near ϕ = 2.3 (in the instance where A = 1), but at this point ($i \approx 30$) the chain segments are less than about 3 monomers in size and the scaling relationship of Eq. (9) has likely become invalid. The square of the entropy change, corresponding to m*, is included in Fig. 5 and compares favorably with the rapidly descending curve fit in Fig. 1 proposed to describe the configurational portion of the master curve. Again, the SAW model is a poor

approximation for the bulk polymer and the purpose of examining this simplistic model is rather to illustrate how the configurational entropy change $dS_{ex}^{*}/d\phi$ could readily develop a decrease with increasing connectivity in qualitative accord with the observation for m^*.

Excess Vibrational Entropy

While it seems intuitive that the configurational entropy would vanish in the vicinity of the rigidity threshold since this marks (in a mean field sense) the connectivity at which the degrees of freedom are first exceeded by an equal number of bonding constraints, it is clear that the reduced fragility does not similarly vanish at this location, but languishes near a value of $m^* = 1$ before appearing to vanish near $\phi = 3$. Thus an additional contribution to S_{ex}^{*} must be active in these over-constrained networks that is non-configurational in origin. Many have alluded to a vibrational contribution[9,27,47] to the excess entropy of the SCL present in addition to the configurational one. Again, this vibrational contribution is one in excess of the crystal's vibrational entropy and is often described as an entropy change associated with a change in the vibrational density of states (DOS) that results when a bonding constraint is removed to produce a local floppy mode at the expense of a higher frequency mode[47]. The vibrational contribution is also thought to be related to the presence of the so-called boson peak[47] - a low energy addition to the DOS beyond that of the Debye manifold that appears to be endemic to amorphous solids. Studies of the boson peak suggest that it is most prominent in strong glassformers[63,64] and, indeed, these are the glass compositions (i.e., $\phi > 2.6$) where the second contribution to m^* is most dominant. Admittedly, this second

contribution is poorly understood at the present time, but the fact that it vanishes for ϕ-networks at $\phi = 3$ is consistent with the expectation that excessively constrained networks, containing a vast number of redundant bonds are less likely to produce a local floppy mode when a bond is randomly removed.

Intermediate Phase

Lastly, we entertain one more experimental finding that supports our proposition that the universal fragility master curve is a consequence of the inherent $dS_{ex}^{*} / d\phi$ of the ϕ-network of weakest linkages. As mentioned in the introduction, studies using temperature-modulated DSC (TMDSC) have revealed a narrow range of NFG compositions near the rigidity threshold whose so-called "non-reversing" heat flow becomes vanishingly small. This non-dissipative feature has lead some to propose that glasses in this compositional range represent an "intermediate phase" comprised of isostatic (rigid but stress-free) networks.

In ordinary DSC experiments, the sample temperature is scanned in a controlled manner while heat flow into or out from the sample is measured. In TMDSC, a temperature modulation is added to the temperature ramp and the heat flow can be separated into reversible and non-reversible contributions[65]. This modulation of temperature drives minor changes in the connectivity that in turn generate changes in the excess entropy that can be approximated by the Taylor expansion:

$$dS_{ex} = \left(\frac{\partial S_{ex}}{\partial \phi}\right)_{\phi} d\phi + \frac{1}{2}\left(\frac{\partial^2 S_{ex}}{\partial \phi^2}\right)_{\phi} \left(d\phi\right)^2 + \cdots . \qquad (13)$$

The first term in the series vanishes over a cycle and represents the reversing part of the heat flow. By contrast, the second term in the series is non-vanishing and represents the non-reversing heat flow that produces a net transfer of heat during the cycle. This non-reversing heat flow would only vanish when the *curvature*, $d^2S_{ex}^*/d\phi^2$, vanishes or, equivalently, at those compositions for which the *slope* of the fragility mastercurve is nearly zero. As seen in Fig. 3, this flattening of the mastercurve corresponds closely with those compositional ranges for which the intermediate phase has been identified.

VI. Conclusion

In summary, we have found a universal dependence of glass fragility on the coarse-grained network connectivity obeyed by over 150 different oxide and non-oxide glass melts. The key to this universality is a broadened definition of the network connectivity that incorporates a coarse-graining of rigid structural units that are present. These rigid units include the short-range ordering endemic to the oxides as well as larger units that reflect the intermediate-range order in some materials. Fragility, which is derived from the temperature dependent viscosity, is a reflection of how the network responds to low frequency deformations and the resulting universality implies that it is only the connectivity of the lattice of weakest linkages that matter to this particular glass-forming metric. From a pragmatic standpoint, the result promises to simplify the processing of glass items from the melt since fragility (together with T_g) defines the viscous response of the melt and can now be determined, in principle, from an intimate knowledge of the glass structure alone. From a broader perspective, the finding underscores the importance of coarse graining when assessing the role of hierarchical

structures in physics. Without the coarse graining, this important tie between melt dynamics and glass structure would otherwise remain hidden.

Acknowledgement: The financial support of NSF (Grant No. DMR-0906640) is gratefully acknowledged.

References

1. W. H. Wang, C. Dong and C. H. Shek, "Bulk metallic glasses," Mat. Sci. and Engg. **R44**, 45-89 (2004).

2. E. Fortunato, P. Barquinha and R. Martins, "Oxide semiconductor thin-film transistors: A review of recent advances," Adv. Mater. **24** (22), 2945-2986 (2012).

3. T. Minami, A. Hayashi and M. Tatsumisago, "Recent progress of glass and glass-ceramics as solid electrolytes for lithium secondary batteries," Solid State Ionics **177**, 2715-2720 (2006).

4. W. E. Lee, M. I. Ojovan, M. C. Stennett and N. C. Hyatt, "Immobilisation of radioactive waste in glasses, glass composite materials and ceramics," Adv. Appl. Ceramics **105**(1), 3 -12 (2006).

5. L. L. Hench, "The story of Bioglass," J. Mater. Sci.: Mater. Med. **17**, 967-978 (2006).

6. J. Zarzycki, Glasses and the vitreous state (Cambridge Univ. Press, 1991).

7. M. D. Ediger and P. Harrowell, "Perspective: Supercooled liquids and glasses," J. Chem. Phys. **137**, 080901 (2012).

8. J. C. Dyre, "Colloquium: The glass transition and elastic models of glass-forming liquids," Rev. Mod. Phys. **78**(3), 953-972 (2006).

9. P. G. Debenedetti and F. H. Stillinger, "Supercooled liquids and the glass transition," Nature **410**, 259-267 (2001).

10. H. Frauenfelder, S. G. Sligar and P. G. Wolynes, "The energy landscapes and motions of proteins," Science **254** (5038), 1598 - 1603 (1991).

11. J. D. Gryngelson, J. N. Onuchic, N. D. Socci and P. G. Wolynes, "Funnels, pathways, and the energy landscape of protein folding: a synthesis," Proteins: Structure, Function, and Bioinformatics **21**(3), 167 - 195 (1995).

12. J. N. Onuchic and P. G. Wolynes, "Theory of protein folding." Current opinion in structural biology, **14**(1), 70 - 75 (2004).

13. M. Goldstein, "Viscous liquids and the glass transition: A potential energy barrier picture," J. Chem. Phys. **31** (9), 3728 - 3739 (1969).

14. F. H. Stillinger, "Supercooled liquids, glass transitions, and the Kauzmann paradox," J. Chem. Phys. **88**(12), 7818 - 7825 (1988).

15. F. H. Stillinger, "A topographic view of supercooled liquids and glass formation," Science **267** (5206), 1935 - 1939 (1995).

16. S. Sastry, P. G. Debenedetti and F. H. Stillinger, "Signatures of distinct dynamical regimes in the energy landscape of a glass-forming liquid," Nature **393** (6685), 554 - 557 (1998).

17. S. Sastry, "The relationship between fragility, configurational entropy and the potential energy landscape of glass-forming liquids," Nature **409** (6817), 164 - 167 (2001).

18. G. Adam and J. H. Gibbs, "On the temperature dependence of cooperative relaxation properties in glass-forming liquids," J. Chem. Phys. **43**, 139 - 146 (1965).

19. G. S. Grest and M. H. Cohen, "Liquids, glasses, and the glass transition: A free-volume approach," Adv. Chem. Phys. **48**, 455- 525 (1981).

20. J. C. Dyre, "Colloquium: The glass transition and elastic models of glass-forming liquids," Rev. Mod. Phys. **78**, 953 - 972 (2006).

21. J. C. Dyre and N. B. Olsen, "Landscape equivalent of the shoving model," Phys. Rev. E **69**, 042501 (2004).

22. R. Richert and C. A. Angell, "Dynamics of glass-forming liquids. V: On the link between molecular dynamics and configurational entropy," J. Chem. Phys. **108**, 9016 - 9026 (1998).

23. S. Corezzi, D. Fioretto, D. Puglia and J. M. Kenny, "Light scattering study of vitrification during the polymerization of model epoxy resins," Macromolecules **36**, 5271 - 5278 (2003).

24. in the original description of the model, only configurational entropy was included. In more recent work, (see e.g., ref. #27) this excess entropy includes also excess vibrational contributions to the entropy.

25. W. Kauzmann, "The nature of the glassy state and the behavior of liquids at low temperatures," Chem. Rev. **43** (2), 219 - 256 (1948).

26. C. A. Angell, "Perspective on the glass transition," J. Phys. Chem. Solids **49** (8), 863-871 (1988).

27. L.-M. Martinez and C. A. Angell, "A thermodynamic connection to the fragility of glass-forming liquids," Nature **410**, 663 - 667 (2001).

28. R. Bohmer, K. L. Ngai, C. A. Angell and D. J. Plazek, "Nonexponential relaxations in strong and fragile glass formers," J. Chem. Phys. **99** (5), 4201 - 4209 (1993).

29. K. Ito, C. T. Moynihan and C. A. Angell, "Thermodynamic determination of fragility in liquids and a fragile-to-strong liquid transition in water," Nature **398**(8), 492 - 495 (1999).

30. W. H. Zachariasen, "The atomic arrangement in glass," J. Am. Chem. Soc. **54** (10), 3841 - 3851 (1932).

31. the reduced fragility on the left-hand side of Eq. 3 is identical with a fragility index introduced in ref. 8 when $m_o = 17$ is replaced $m_o = 16$.

32. J. C. Phillips, "Topology of covalent non-crystalline solids I: Short-range order in chalcogenide alloys," J. Non-Cryst. Solids, **34**, 153-181 (1979).

33. H. He and M. F. Thorpe, "Elastic properties of glasses," Phys. Rev. Lett. **54**, 2107-2110 (1985).

34. M. F. Thorpe, D. J. Jacobs, N. V. Chubynsky and A. J. Rader, "Generic rigidity of network glasses," in Rigidity Theory and Applications, ed. by Thorpe and Duxbury (Kluwer Acad./Plenum, 1999). p. 239 -277.

35. J. C. Mauro, "Topological constraint theory of glass," Am. Ceram. Soc. Bull. **90** (4) 31 -37 (2011).

36. P. K. Gupta and J. C. Mauro, "Composition dependence of glass transition temperature and fragility. I. A topological model incorporating temperature-dependent constraints," J. Chem. Phys. **130** (9), 094503 (2009).

37. M. Tatsumisago, B. L. Halfpap, J. L. Green, S. M. Linsey and C. A. Angell, "Fragility of Ge-As-Se glass-forming liquids in relation to rigidity percolation and the Kauzmann paradox," Phys. Rev. Lett. **64** (13), 1549 (1990).

38. R. Boehmer and C. A. Angell, "Correlations of the noexponentiality and state dependence of mechanical relaxations with bond connectivity in Ge-As-Se supercooled liquids," Phys. Rev. B **45** (17), 10091 (1992).

39. P. Boolchand, D. G. Georgiev and B. Goodman, "Discovery of the intermediate phase in chalcogenide glasses," J. Optoelectronics Adv. Mat. **3** (3), 703 - 720 (2001).

40. M. Micoulaut and J. C. Phillips, "Rings and rigidity transitions in network glasses," Phys. Rev. B **67**, 104204 (2003).

41. C. A. Angell and K. J. Rao, "Configurational excitations in condensed matter and the "bond lattice" model for the liquid-glass transition," J. Chem. Phys., **57**, 470-481 (1972).

42. R. Fabian, Jr. and D. L. Sidebottom, “Dynamic light scattering in network-forming sodium ultraphosphate liquids near the glass transition”, *Phys. Rev. B* **80**, 064201 (2009).

43. Tri D. Tran and D. L. Sidebottom, “Glass-forming dynamics of aluminophosphate melts studied by photon correlation spectroscopy", *J. Am. Ceram. Soc.* **96**, 2147 (2013).

44. A. B. Seddon, "Chalcogenide glasses: A review of their preparation, properties and applications," J. Non-cryst. Solids **184**, 44 - 50 (1995).

45. D. L. Sidebottom and S. E. Schnell, "The role of intermediate range order in predicting fragility of network-forming liquids near the rigidity transition," Phys. Rev. B **87**, 054202 (2013).

46. D. L. Sidebottom, T. D. Tran and S. E. Schnell, "Building up a weaker network: The effect of intermediate range glass structure on liquid fragility," J. Non-Cryst. Sol. **402**, 16 - 20 (2014).

47. C. A. Angell and C. T. Moynihan, "Ideal and cooperative bond-lattice representations of excitations in glass-forming liquids: Excitation profiles, fragilities, and phase transitions", Metallurgical and Materials Trans. **31B**, 587 - 596 (2000).

48. D. L. Griscom in Borate Glasses: Structure, properties and applications *Materials Science Research*, vol. 12, edited by L. D. Pye, V. D. Frechette and N. J. Kreidel (Plenum, New York, 1978).

49. R. E. Youngman and J. W. Zwanziger, "Network modification in potassium borate glasses: structural studies with NMR and Raman spectroscopies," J. Phys. Chem. **100**, 16720 - 16728 (1996).

50. Y. Yang, B. Zhang, A. Yang, Z. Yang, and P. Lucas, "Structural origin of fragility in Ge-As-S glasses investigated by calorimetry and Raman spectroscopy," J. Phys. Chem. B **119** (15), 5096 - 5101 (2015).

51. G. Yang, O. Gulbiten, Y. Gueguen, B. Bureau, J.-C. Sangleboeuf, C. Roiland, E.A. King and P. Lucas, "Fragile-strong behavior in the As_xSe_{1-x} glass forming system in relation to structural dimensionality," Phys. Rev. B **85**(14), 144107(8) (2012).

52. T. Wang, O. Gulbiten, R. Wang, Z. Yang, A. Smith, B. Luther-Davies, and P. Lucas, "Relative contribution of stoichiometry and mean coordination to the fragility of Ge-As-Se glass forming liquids," J. Phys. Chem. B **118** (5), 1436-1442 (2014).

53. S. Sen and B. G. Aitken, "Atomic structure and chemical order in Ge-As selenide and sulfoselenide glasses: An X-ray absorption fine structure spectroscopic study," Phys. Rev. B: Condens. Matter **66**, 134204 (2002).

54. G. Yang, B. Bureau, T. Rouxel, Y. Gueguen, O. Bulbiten, C. Roiland, E. Soignard, J. Y5rger, J. Troles, J.-C. Sangleboeuf, and P. Lucas, "Correlation between structure and physical properties of chalcogenide glasse in the As_xSe_{1-x} system," Phys. Rev. B **82**, 195206 (2010).

55. B. G. Aitken and C. W. Ponader, "Physical properties and Raman spectroscopy of GeAs sulphide glasses," J. Non-Cryst. Sol. **256/257**, 143 - 148 (1999).

56. B. G. Aitken and C. W. Ponader, "Property extrema in GeAs sulphide glasses," J. Non-Crsyt. Sol. **274**, 124 - 130 (2000).

57. S. Sugai, "Stochastic random network model in Ge and Si chalcogenide glasses," Phys. Rev. B **35** (3) 1345 -1361 (1987).

58. T. G. Edwards and S. Sen, "Structure and relaxation in germanium selenide glasses and supercooled liquids: A Raman spectroscopic study," J. Phys. Chem. B **115**, 4307 - 4314 (2011).

59. B. G. Aitken, "GeAs sulfide glasses with unusually low network connectivity," J. Non-Cryst. Solids **345/346**, 1-6 (2004).

60. A. J. Guttmann and A. R. Conway, "Square lattice self-avoiding walks and polygons", Annals of Combinatorics **5**, 319- 345 (2001).

61. D. MacDonald, S. Joseph, D. L. Hunter, L. L. Moseley, N. Jan and A. J. Guttmann, "Self-avoiding walks on the simple cubic lattice", J. Phys. A: Math. Gen. **33**, 5973 - 5983 (2000).

62. R. D. Schram, G. T. Barkema and R. H. Bisseling, "Exact enumeration of self-avoiding walks", J. Stat. Mech.: Theory and Expt. **2011** (6), P06019 (2011).

63. M. D. Ediger, C. A. Angell and S. R. Nagel, "Supercooled liquids and glasses", J. Phys. Chem. **100**, 13200 - 13212 (1996).

64. A. P. Sokolov, E. Rossler, A. Kisliuk and D. Quitmann, "Dynamics of strong and fragile glass formers: Differences and correlations with low-temperature properties." Phys. Rev. Lett. **71**(13), 2062 - 2065 (1993).

65. J. E. K. Schawe, "Principles for the interpretation of temperature-modulated DSC measurements. Part 2: A thermodynamic approach," Thermochimica Acta **304/305**, 111-119 (1997).

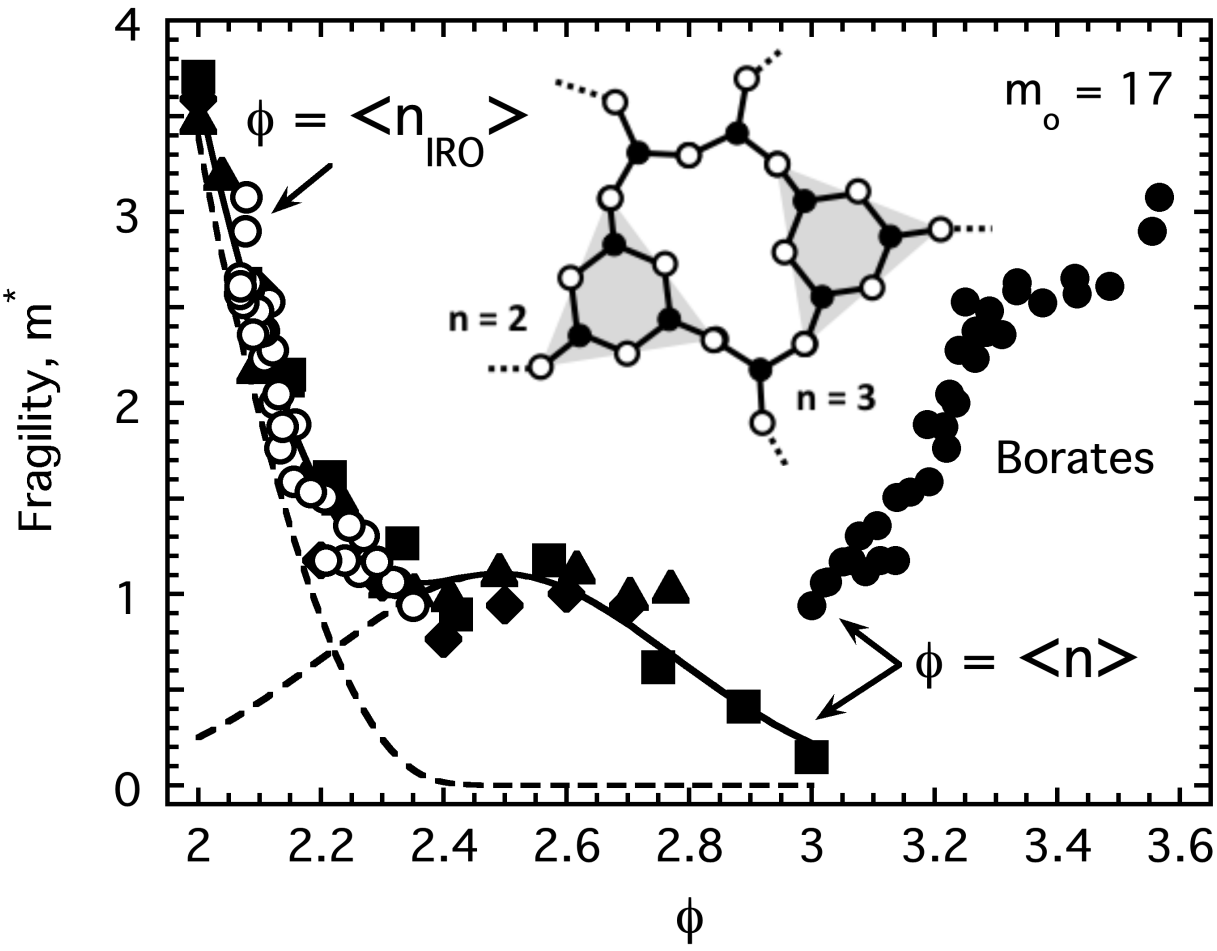

Figure 1: The reduced fragility of $Ge_xAs_xSe_{1-2x}$ (diamonds with $\phi = \langle r \rangle$), $(Na_2O)_x(P_2O_5)_{1-x}$ (squares with $\phi = \langle n \rangle$), $(Al(PO_3)_3)_x(NaPO_3)_{1-x}$ (triangles with $\phi = \langle n \rangle$) and $(M_2O)_x(B_2O_3)_{1-x}$ (solid circles with $\phi = \langle n \rangle$ and open circles with $\phi = \langle n_{IRO} \rangle$) plotted against the connectivity, ϕ. Here the fragility has been reduced using $m_o = 17$. Two dashed lines indicate a curve fit combining a quadratic function that vanishes at 2.4 and a Gaussian centered near 2.5. The inset shows a snippet of the boron glass structure illustrating the boroxol ring and its reduced connectivity.

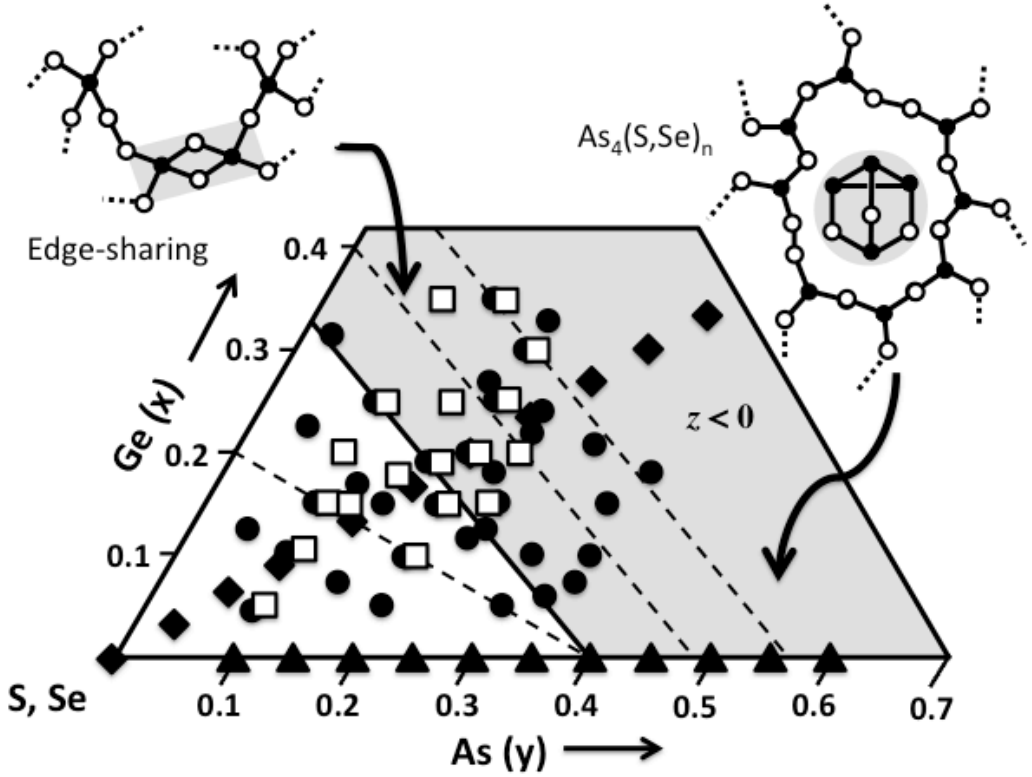

Figure 2: A truncated ternary phase diagram showing all the chalcogenide compositions under investigation. Solid symbols are $Ge_xAs_ySe_{1-x-y}$. Open squares are $Ge_xAs_yS_{1-x-y}$. Data are taken from reference [51] (triangles), reference [37,38] (diamonds), reference [52] (circles) and reference [50] (squares). The solid line connecting between the two binaries marks the location of compositions with $z = 0$. Two dashed lines parallel to this mark the location of compositions with $z = -0.2$ and -0.4, respectively. The remaining dashed line in the region $z > 0$ locates compositions with $\langle r \rangle = 2.4$. The inset in the upper left depicts edge-sharing tetrahedral units found in the Ge-rich region at $z < 0$. The inset in the upper right depicts an $As_4(S,Se)_3$ molecule trapped in a network void.

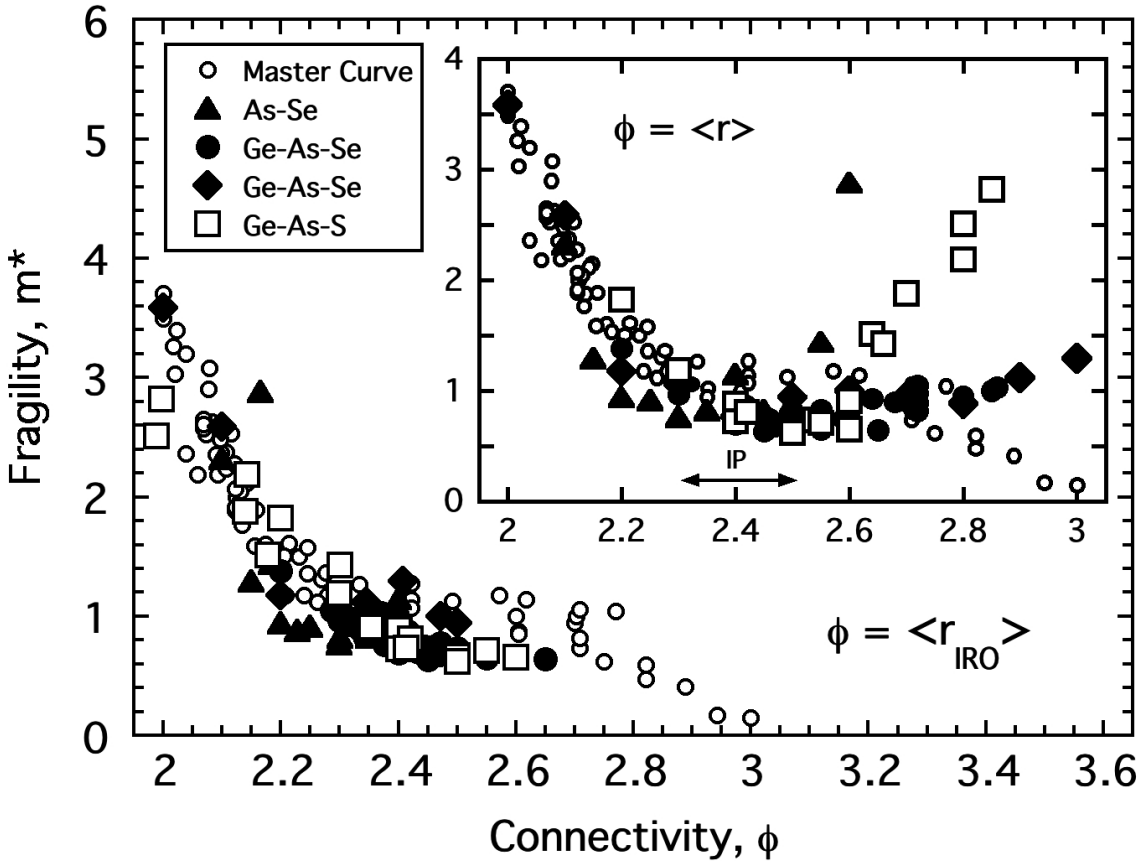

Figure 3: The reduced fragility (m_o = 17) of 153 different oxide and non-oxide glasses combined to form a mastercurve as a function of the coarse-grained connectivity of the network. Open circles are various oxide glasses reported previously[46]. Other symbols are as defined for Figure 2. Inset shows the same reduced fragility of the chalcogenide glasses when plotted using the average bond per atom, $\phi = \langle r \rangle$. The intermediate phase (IP) is typically found in a range between $\langle r \rangle$ = 2.3 and 2.5.

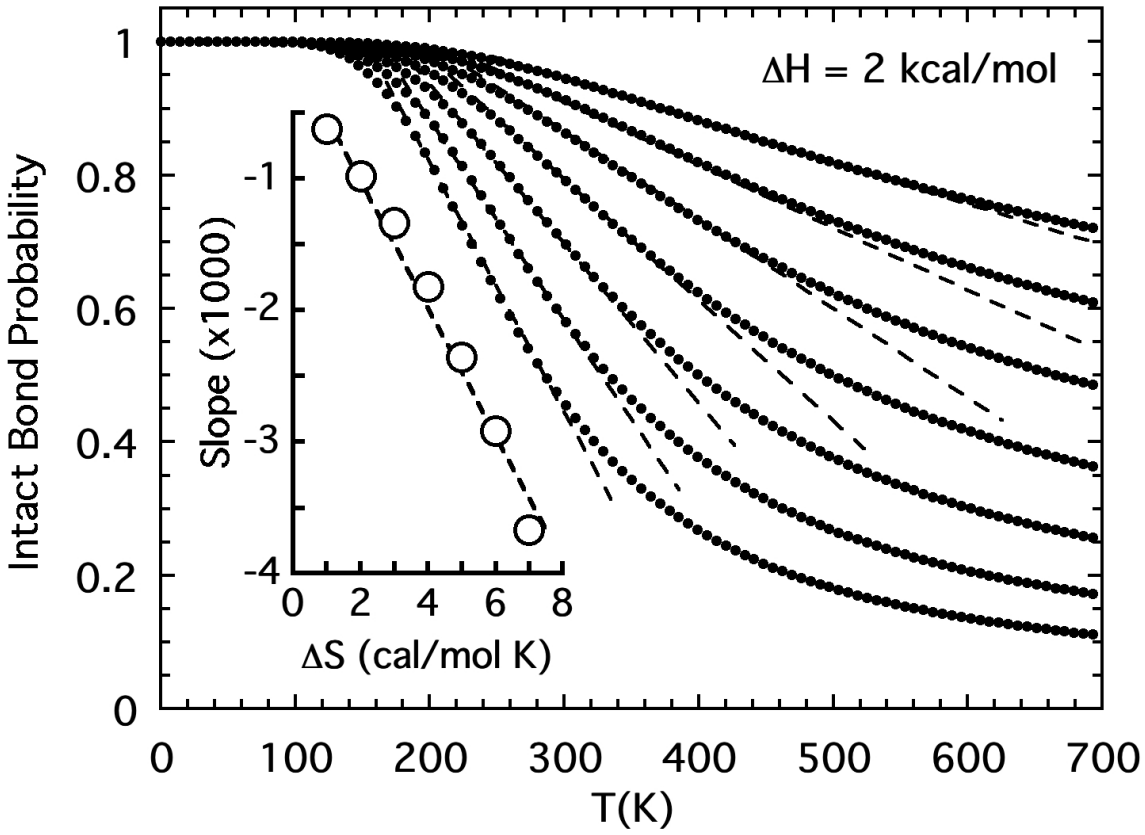

Figure 4: The intact bond probability for a two state model using fixed ΔH = 2 kcal/mol and a selection of ΔS = 1 to 7 cal/mol K. Regions of linear temperature dependence are highlighted by the dashed lines. Inset shows the slope of the dashed lines and its rough proportionality with the value of ΔS.

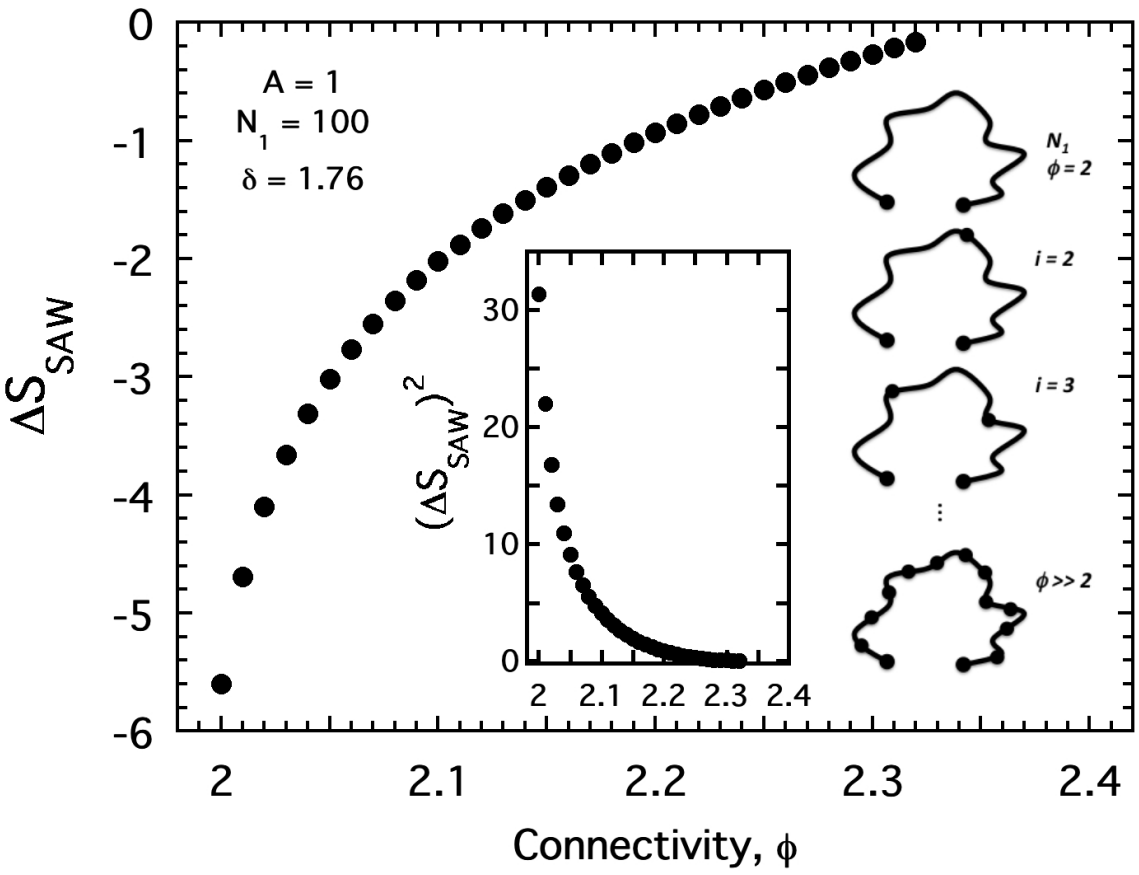

Figure 5: The change in configurational entropy, ΔS_{SAW}, obtained from Eq. (12) for the constrained SAW polymer coil discussed in the text, is plotted against the connectivity given by Eq. (11). Inset shows the same quantity squared as well as illustrations of how the initial polymer coil is sequentially constrained by added crosslinks.